Microchimica Acta (2021) 188: 346
https://doi.org/10.1007/s00604-021-04967-y

ORIGINAL PAPER

DNA dendrimer–templated copper nanoparticles: self-assembly, aggregation-induced emission enhancement and sensing of lead ions

Min Li[1] · Yi-Na Cai[2] · Chi-Fang Peng[1,3,4] · Xin-Lin Wei[5] · Zhou-Ping Wang[1,3,4]

Received: 1 May 2021 / Accepted: 30 July 2021 / Published online: 19 September 2021

Abstract

Copper nanomaterials based on DNA scaffold (DNA-Cu NMs) are becoming a novel fluorescent material, but it is still challenging to obtain highly fluorescent DNA-Cu NMs with excellent stability. In this work, we report a kind of copper nanoassemblies (Cu NASs) with aggregation-induced emission enhancement (AIEE) property using DNA dendrimers with sticky end as template. The sticky end of the DNA dendrimers induced the formation of much bigger Cu NASs with average size ranging from 131 to 264 nm, depending on the length of the DNA dendrimer sticky end from 6 bases to 27 bases. Compared with complete complementary DNA dendrimer, nearly 6-fold fluorescence enhancement was achieved using DNA dendrimer with 27 bases sticky end. Moreover, the DNA dendrimer-Cu NASs demonstrated excellent stability in serum and could be rapidly quenched by Pb^{2+} ions. Based on the above property, highly sensitive and selective fluorescent detection of Pb^{2+} ions was possible with a linear range of 2.0–100 nM and a detection limit of 0.75 nM. Due to the sensitive and rapid response to Pb^{2+} as well as excellent stability in complex matrix, the proposed fluorescent Cu NASs demonstrated high potential as an excellent fluorescent probe for Pb^{2+} in complex matrix.

Keywords Copper nanocluster · Self-assembly · Nucleic acids · Fluorescence detection · Aggregation-induced emission enhancement · Lead determination

Introduction

Fluorescent metal nanomaterials (NMs), including metal nanoparticles (Cu NPs) and metal nanoclusters (Cu NCs), have attracted much attention and have been widely used in molecular recognition and other biomedical studies owing to their low toxicity, ultrasmall size, and tunable fluorescent properties [1, 2]. However, the quantum yields (QYs) of water-dispersible fluorescent NMs are normally lower than those well-established inorganic quantum dots [3, 4]. The shortcoming greatly limits their optical applications.

More recently, aggregation-induced emission enhancement (AIEE) phenomenon has been observed in many metal NMs [5], which is similar as the organic chromophore [6]. Some AIEE NMs have been prepared via structure-induced lipophilic self-assembly [7], ion or solvent-induced self-assembly [8], and peptide-induced aggregation self-assembly [9]. Based on the AIEE property, some gold (Au), silver (Ag), and copper (Cu) NMs have been successfully applied in environmental [10] and biochemical analyses [11]. Among these noble metallic NMs, Cu NMs is relatively earth-abundant and cost-effective. Many templates, such as polymers, peptides and proteins, small molecules, and DNA [12], can be used to synthesize Cu NMs. DNA scaffold–templated

✉ Chi-Fang Peng
pcf@jiangnan.edu.cn

✉ Zhou-Ping Wang
wangzp@jiangnan.edu.cn

[1] State Key Lab of Food Science and Technology, Jiangnan University, Wuxi 214122, People's Republic of China

[2] Inspection and Quarantine Technology Centre, Shenzhen Customs, Shenzhen 518045, People's Republic of China

[3] School of Food Science and Technology, Jiangnan University, Wuxi 214122, People's Republic of China

[4] National Engineering Research Center for Functional Food, Jiangnan University, Wuxi 214122, People's Republic of China

[5] School of Agriculture and Biology, Shanghai Jiaotong University, Shanghai 200240, People's Republic of China

Cu NMs (DNA-Cu NMs) have also raised much concern in terms of their molecular recognition and have been used in biomedical applications [13, 14]. Nevertheless, most fluorescent DNA-Cu NMs could keep stable for only a few hours [15]; it is still highly challenging to prepare highly fluorescent Cu NMs with excellent stability in complex matrix. Since single- and double-stranded DNA can be easily degraded in biological matrix, the damage of DNA templates will decrease the stability of these DNA-Cu NMs and the application repeatability [16]. Thus, the preparation of fluorescent DNA-Cu NMs with high stability is very important for their applications in sensing method against analytes in complex matrix.

DNA strands have been successfully used to assist various nanomaterials' self-assembly due to the programmable synthesis, spatial addressability, and powerful molecular recognition [17]. But up to now, very limited study on AIEE Cu NMs has been reported using DNA scaffold as template. Lately, DNA nanoribbons, containing multiple specific binding sites, served as a template for successful synthesis and assembly of ultrasmall Cu NMs [18]. Dendritic DNA nanostructures demonstrated highly potential applications in biomedicine and biotechnology on the basis of their monodispersity, excellent stability, and highly branched structures [19]. DNA dendrimer as template might also enhance fluorescence emission and stability of Cu NMs [18].

Herein, highly fluorescent Cu nano-assemblies (Cu NASs) were prepared using DNA dendrimers with sticky end as template for the first time. The sticky end of the DNA dendrimers was found to significantly affect the size, fluorescent intensity, and stability of the Cu NASs. Mono-dispersed over 100 nm Cu NASs could be obtained through self-assembly of Cu NCs initiated by the sticky end of the DNA dendrimers as illustrated in Fig. 1. The Cu NASs demonstrated not only significant AIEE property, but also excellent stability in biological matrix. Moreover, the above fluorescent Cu NASs can be used as an excellent fluorescent probe for lead ions (Pb^{2+}) in biological matrix.

Experimental

Materials and instruments

All of the oligonucleotide acids were synthesized by Shanghai Sangon Biotechnology Co., Ltd. (Shanghai, China, https://www.sangon.com/), and their sequences are shown in Table S1. Rhodamine 6G was purchased from Aladdin Reagent Company (Shanghai, China, https://www.aladdin-e.com/). Fetal bovine serum (FBS) was obtained from Fisher Scientific Ltd. (Beijing, China, http://www.wissen-bio.com), and 3-(N-morpholino) propanesulfonic acid (MOPS), ascorbic acid (AA), NaAc, sodium hydroxide (NaOH), $Cu(Ac)_2$, $Pb(Ac)_2$, $MgCl_2$, and other used metal salts were purchased from Sinopharm Chemical Reagent Co., Ltd. (Shanghai, China, https://www.sinoreagent.com/). All of other chemicals were analytical grade. The water used in all experiments was ultrapure water.

Transmission electron microscopy (TEM) images were obtained on a JEOL JEM-2100 transmission electron microscope (Hitachi, Japan) with a working voltage of 200 kV. UV-vis absorption spectroscopic measurements were carried out using a microplate reader (Elx800, BioTek Instruments, USA). Dynamic light scattering (DLS) analyses were carried out on a NanoBrook Omni apparatus (Brookhaven Instruments, USA). All fluorescence measurements were performed using a fluorescence spectrophotometer F97Pro (Shanghai Lengguang Technology, China) with quartz cuvette. The excitation wavelength was fixed at 340 nm with both excitation and emission bandwidths set at 5.0 nm. X-ray photoelectron (XPS) measurements were made on an Escalab 250Xi spectrometer (Thermo Scientific, USA). The fluorescent quantum yield (QY) of the Cu NASs was measured by a reference method using Rhodamine 6G as reference fluorescent dye (QY=95%). Fluorescence lifetime measurements were measured using a FLS980 fluorescence spectrometer (Edinburgh Instruments, UK). Transmission electron microscope (TEM) and high-angle annular dark-field scanning transmission electron microscopy (HAADF-STEM) images, selective area electron diffraction (SAED) pattern, and

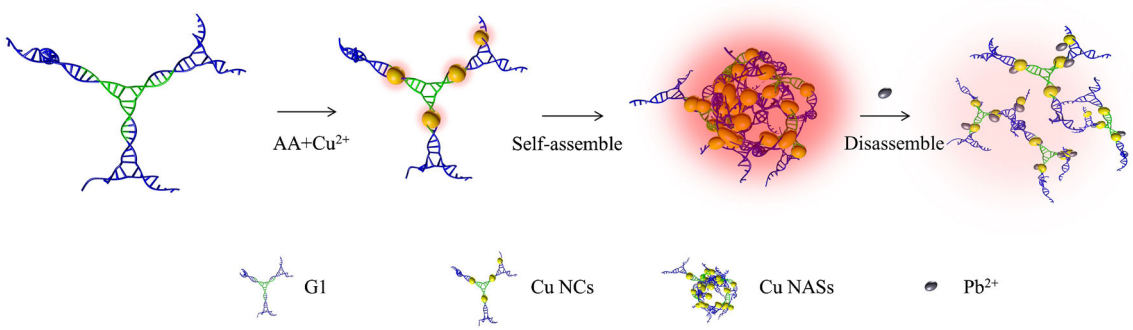

Fig. 1 Schematic diagram of the preparation of DNA dendrimer-Cu NASs and Pb^{2+} sensing

energy-dispersive X-ray spectroscopy (EDS) elemental mapping of nanoparticles were obtained on a Tecnai G20 microscope (FEI, USA).

Preparations of Cu NASs

Fluorescent Cu NASs were synthesized according to the reported method with slight modification [19, 20]. DNA dendrimers were prepared using building blocks of Y-shaped junction scaffolds (Y-DNA). Three oligonucleotide strands (Y0a, Y0b, Y0c; see Table S1 in Supporting Information) were equally mixed in MOPS buffer (10 mM, pH 7.5, 150 mM NaAc, 1 mM $MgCl_2$). The mixed solution was heated to 90°C and slowly cooled down to 4°C. The annealed sample was incubated for an additional 30 min at room temperature to obtain a Y-shaped DNA building block (Y0). Another Y-shaped DNA building block (Y1) was also prepared with three different oligonucleotides strands through similar steps. Y1 also have three duplex arms with 13 bases pairs with or without single-stranded sticky end. Y0 and Y1 with sticky end (X bases) were named as Y0-SteX and Y1-SteX (Fig. S1). Y0 and Y1 can hybrid through their complementary sticky ends in a ratio of 1 to 3 and then the DNA dendrimers (named as G1) were obtained. For the sake of description, Y0-SteX also was named as G0-SteX.

Then, the DNA dendrimer (G1, 500 μL, 500 nM) was mixed with AA dissolved in MOPS buffer (500 μL, 1.25 mM), followed by the immediate addition of $Cu(Ac)_2$ dissolved in ultrapure water (200 μL, 500 μM). The above solutions were mixed well for 20 min to complete the self-assembly from Cu NC to G1-Ste13 Cu NASs. The effect of the buffer pH and Cu^{2+} concentration was also investigated. The obtained nanomaterials were stored in the dark at 4 °C for the next experiments.

Fluorescence detection of Pb^{2+} ions

In a typical detection, 980 μL of 62.5 nM (G1) Cu NASs was incubated with 20 μL Pb^{2+} ions in MOPS buffer (10 mM, pH 7.5, 150 mM NaAc, 1 mM $MgCl_2$) for 20 min. After incubation, the fluorescence spectra of the Cu NASs system were scanned by a fluorescence spectrometer under 340-nm excitation.

The selectivity toward other common metal ions was tested. First, 980 μL of Cu NASs was mixed with 20 μL of various metal ions (Al^{3+}, Ba^{2+}, Fe^{3+}, Ca^{2+}, Cd^{2+}, Hg^{2+}, Cu^{2+}, Ni^{3+}, Co^{2+}, Mg^{2+}, Mn^{2+}, Zn^{2+}, Pb^{2+}), respectively. After being incubated for 20 min, the fluorescence quenching was analyzed. All of the measurements were performed three times, and the standard deviation was plotted as an error bar. In the stability analysis, 100 uL Cu NASs or dsDNA-Cu NCs (500 nM) was added to 700 uL FBS to observe the fluorescence change.

Detection of Pb^{2+} in real samples

In order to investigate the practical application of the fluorescent probe in real samples, FBS were spiked with various concentrations of Pb^{2+} (0.1, 0.4, and 1.6 mM) and tested by the above method. After the addition of Pb^{2+}, the FBS samples were centrifuged at 10,000 rpm for 20 min. The obtained serum supernatants were diluted with MOPS buffer (10 mM, pH 7.5) by 20-fold and then incubated with the Cu NASs for 20 min. Finally, the fluorescence emission was measured. The calculation of recovery was according to the standard curve and equation: Recovery (%) = detected Pb^{2+} concentration/spiked Pb^{2+} concentration. The detected Pb^{2+} concentration was calculated according to the corresponding fluorescent signal and the standard curve.

Results and discussion

Characterization of Cu NASs

The effect of buffer pH and Cu^{2+} concentration on the Cu NASs preparation was investigated. As shown in Fig. S2, the brightest signal of fluorescent Cu NASs was obtained at pH 7.5 and 500 μM Cu^{2+}. Since the size of DNA templates could play a key role in the Cu NMs preparation [15], DNA dendrimers (G0-Ste13 and G1-Ste13) were compared firstly. As shown in Fig. S3, G1-Ste13-Cu NMs demonstrated hyperchromic shift at 340 nm in the UV-vis spectra and 1.6-fold fluorescent enhancement compared with G0-Ste13-Cu NMs. Then, the length of sticky end in the G1 was investigated carefully. As shown in Fig. 2a, the UV-vis absorption of the DNA dendrimer G1 templated Cu NMs showed hyperchromic shift at 340 nm with the increasing length of the G1 sticky end from 0 to 27 bases. These results indicated that the size of DNA dendrimer–templated Cu NMs increased with the increasing size of DNA dendrimer templates since increased nanoparticles would result in background scattering [21, 22]. These Cu NMs exhibited red fluorescence under UV light while colorless under visible light (Fig. 2b). The excitation and emission peaks of Cu NASs were located at 340 nm and 590 nm (Fig. S3), which were similar to the previous results [20]. Interestingly, the fluorescent intensity of the Cu NMs increased gradually with the increasing length of the sticky end of G1 from 0 to 27 bases and nearly 6-fold enhancement was achieved (Fig. 2b).

The TEM images demonstrated that the much-packed morphology and ordered arrangement appeared in the Cu NASs as the prolonged sticky end of G1 was introduced (Fig. 3). In general, the sizes of the Cu NASs were much bigger than that of the dendrimer DNA template (Fig. S4). The average size of G1-Ste0-Cu NCs was 19 nm. As the base number of G1 sticky ends increased to 6, 13, 20, and 27, the average size of the Cu

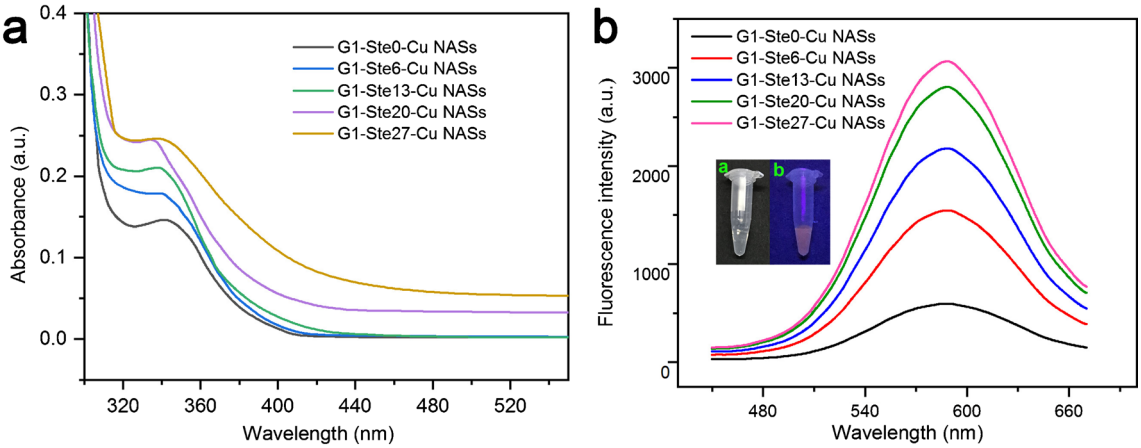

Fig. 2 **a** UV-vis absorption spectra of G1-Ste0-Cu NASs, G1-Ste6-Cu NASs, G1-Ste13-Cu NASs, G1-Ste20-Cu NASs, and G1-Ste27-Cu NASs. **b** Fluorescent spectra of G1-Ste0-Cu NASs, G1-Ste6-Cu NASs, G1-Ste13-Cu NASs, G1-Ste20-Cu NASs, and G1-Ste27-Cu NASs. Inset: photographs of the G1-Ste13-Cu NASs under natural light (a) and UV light (b)

NASs increased from 19 to 131 nm, 160 nm, 220 nm, and 264 nm, respectively (Fig. S4a), while the size of templates was estimated to be about 18 nm, 21 nm, 21 nm, 23 nm, and 25 nm, respectively (Fig. S4b). These results indicated that the formation of these Cu NASs consisted of two processes: dendrimer DNA–templated Cu NCs growth and single DNA strand–driven self-assembly of DNA-Cu NCs (Fig. 1). The previous work revealed that the Cu NCs were accumulated in the major groove of the dsDNA [20]. Due to the rigid structure of dsDNA, dsDNA template cannot fully coat the surface in dsDNA-templated Cu NCs preparation. But the sticky end of the dendrimer DNA template in the Cu NCs could be absorbed easily onto the surface of Cu NCs, which may be the main driving force in the self-assembly of DNA-Cu NCs [23]. It can also be observed that when there was the same number of bases in the DNA template, the degree of self-assembly of G0-Ste13-Cu NASs (template with 3 sticky ends) was weaker than that of G1-Ste13-Cu NASs (template with 6 sticky ends), and its smaller particle size and looser spherical density indicate the influence of sticky ends on self-assembly,

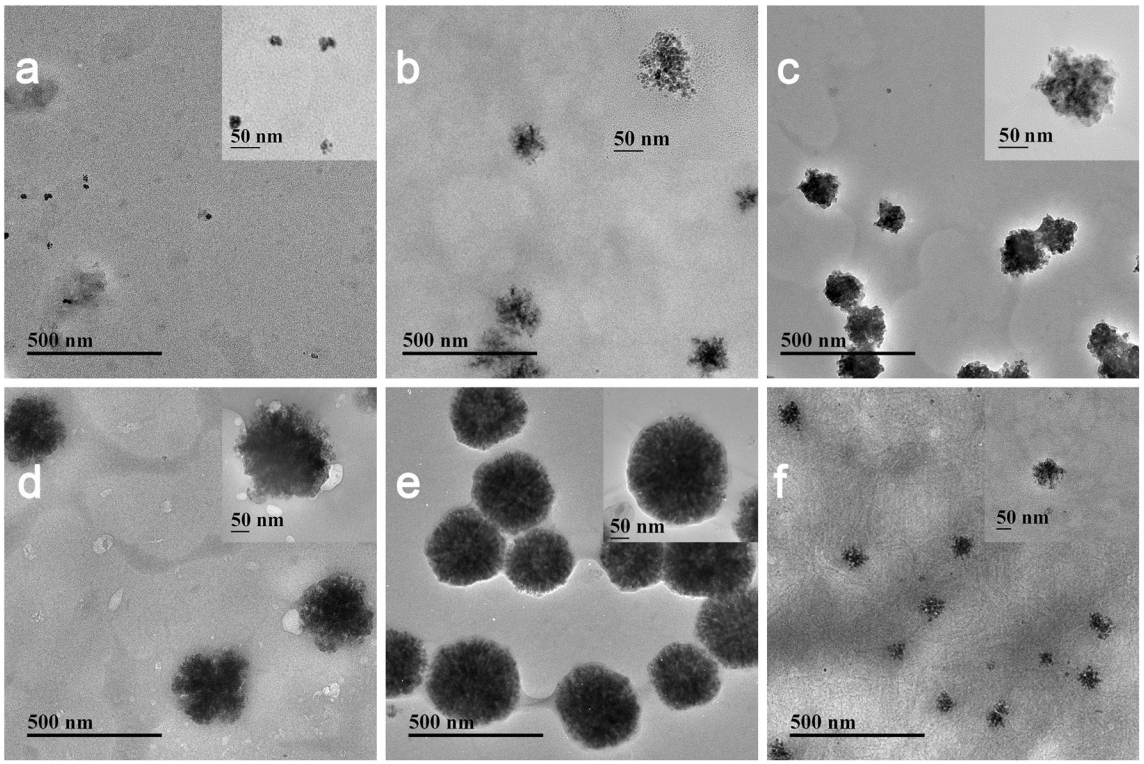

Fig. 3 TEM images of **a** G1-Ste0-Cu NASs, **b** G1-Ste6-Cu NASs, **c** G1-Ste13-Cu NASs, **d** G1-Ste20-Cu NASs, **e** G1-Ste27-Cu NASs, and **f** G0-Ste13-Cu NASs

but its particle size was still larger than G0-Ste13 (Fig. 3f and Fig. S4)

HAADF-STEM image and corresponding elemental mappings showed that Cu, C, N, and P elements were densely and uniformly distributed in the G1-Ste13-Cu NASs, which was consistent with the morphology of the G1-Ste13-NASs (Fig. 4a, Fig. 4b, and Fig. 4c). The lattice fringes with 0.208-nm lattice space ascribed to (111) planes of Cu can be clearly observed in the HRTEM image (Fig. 4d) [24]. Furthermore, SAED pattern of the hydrangea nanostructure exhibited polycrystalline diffraction rings (Fig. 4e), which revealed that the G1-Ste13-Cu NASs was polycrystalline structures [25].

To better understand the mechanism of fluorescence enhancement of the Cu NASs, we conducted fluorescence lifetime measurement for G1-Ste0-Cu NASs and G1-Ste13-Cu NASs. The fluorescence lifetime of G1-Ste0-Cu NASs was 9.2 ns (calculated from two individual lifetimes of 0.63 ns (0.02%) and 9.27 ns (99.98%)). After increasing the length of sticky end in the G1, the average lifetime of G1-Ste13-Cu NASs was increased to 14 ns (Fig. S5, Table S2). Combining with the compact morphology and the long fluorescence lifetime, the fluorescence intensity increase after Cu NCs self-assembly should relate to the suppression of intramolecular vibration and rotation of surface ligands on the Cu NCs, leading to decreased nonradiation and increased fluorescence emission [4, 26, 27]. The dependency of the fluorescence intensity on the size and morphology of Cu NASs confirmed that strong AIEE effect existed in the fluorescent Cu NASs. And the phenomenon of AIEE for Cu NCs has been recently reported [5, 28].

Using Rhodamine 6G as reference, the quantum yields (QY) of Cu NASs were measured [29, 30]. As the sticky end of G1 increased from 0 to 27, the QY of G1-Cu NCs and G1-Cu NASs increased from 4 to 17% (Table S3). These results demonstrated that the QY of dendrimer DNA-Cu NASs could be well-controlled by tailoring the sticky end of dendrimer DNA template.

The dendrimer DNA-Cu NASs and dsDNA-Cu NCs were incubated in serum for days and then fluorescence changes were measured. The results showed that the fluorescence

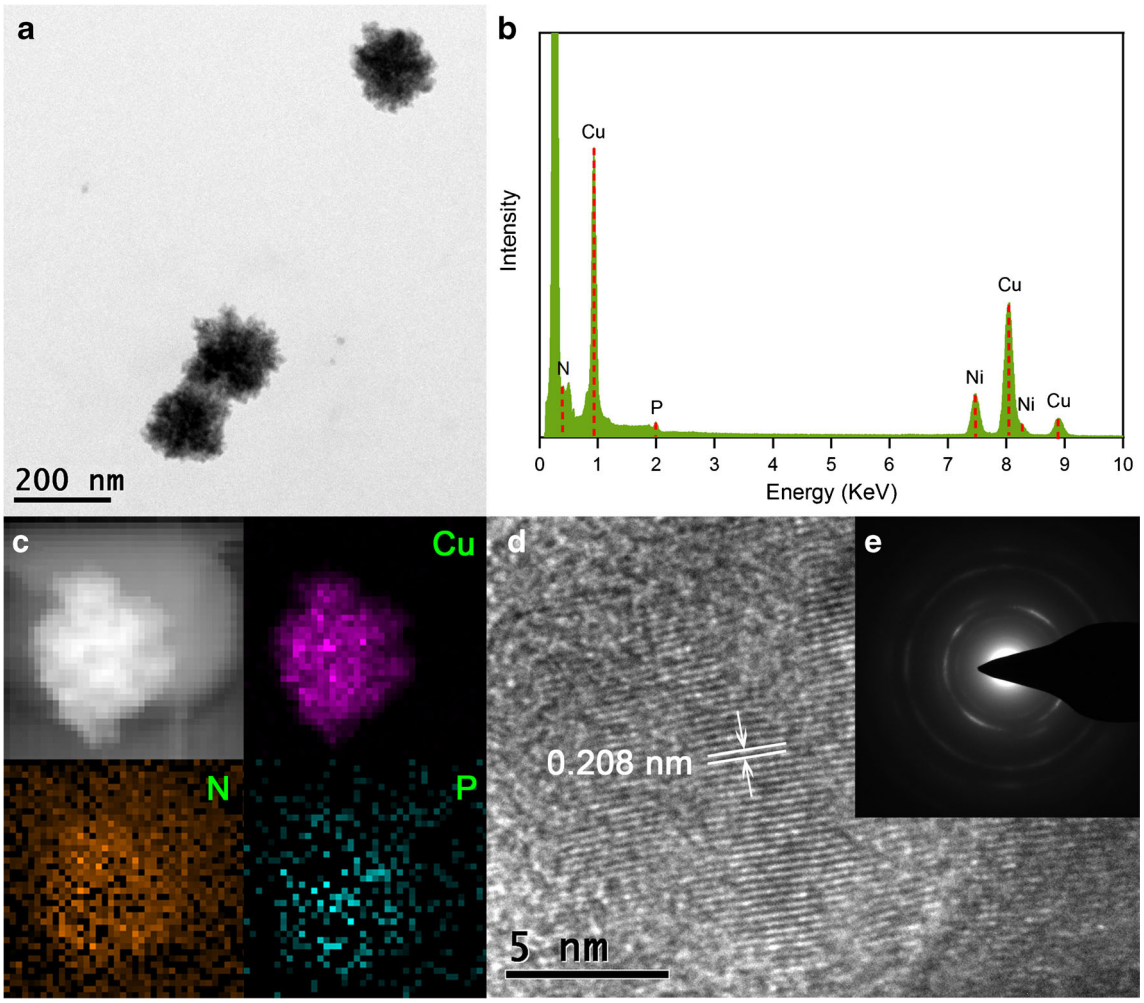

Fig. 4 **a** TEM image, **b** EDS spectrum, **c** HAADF-STEM EDS elemental mapping, and **d** HRTEM image of the G1-Ste13-Cu NASs. Inset of **e** represents corresponding SAED patterns

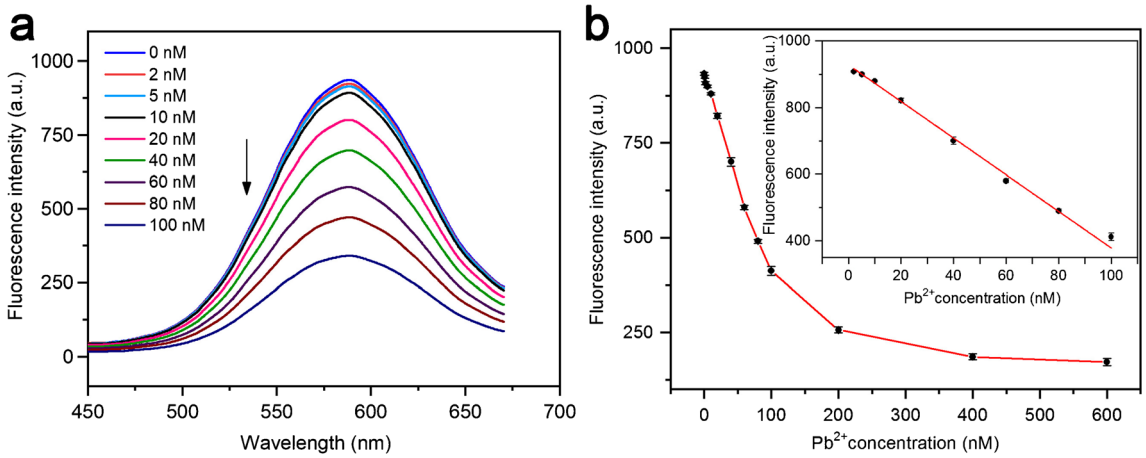

Fig. 5 **a** Fluorescence spectral changes of G1-Ste13-Cu NASs upon addition of Pb^{2+}; **b** the fluorescence intensity against Pb^{2+} concentration. The inset is the fluorescence quenching of the Cu NASs by Pb^{2+} in the range of 0–100 nM. (λex = 340 nm, λem = 590 nm)

intensity of the G1-Ste13-Cu NASs barely changed after being stored with serum for 6 days. However, the dsDNA-templated Cu NCs only kept stable for 4 h and only 24% fluorescence intensity was preserved after 1 day (Fig. S6). This was due to that reticular DNA structure finally formed in the dendrimer DNA–templated Cu NASs and this kind of DNA structure was much more resistant to nuclease degradation than common DNA structure [19, 31].

Analytical performance of Pb^{2+} sensing

Pb^{2+} is one of hazardous heavy metal ion, seriously threatening the environment and human health due to their long-term accumulation in the human body [32]. Zeng and co-workers developed the detection of Pb^{2+} with high selectivity and sensitivity using DNA-templated copper NCs as fluorescence probe in aqueous solution [20]. Despite their excellent results, to the best of our knowledge, no work on Cu NASs with AIEE property as fluorescent probe for Pb^{2+} detection was reported so far.

To achieve sensitive detection for Pb^{2+} ions, dendrimer DNA-Cu NASs with sticky end of various lengths were compared. The G1-Ste13-Cu NASs with 13 bases of sticky end were found to be the most sensitive probe to Pb^{2+} detection (Fig. S7a). This was mainly due to that the fluorescence emission will be enhanced when the sticky end of the Cu NASs was prolonged. However, when the sticky end was too long, the structure of the Cu NASs became denser. The denser structure will hinder the combination of Pb^{2+} and Cu NASs to some extent.

The dilution of the G1-Ste13-Cu NASs was investigated and the results showed that 8-fold dilution of the G1-Ste13-Cu NASs was most sensitive to Pb^{2+} ions (Fig. S7b). Moreover, the G1-Ste13-Cu NASs could be quenched rapidly by Pb^{2+} ions. Obvious fluorescence change could be detected in 5 min and highest fluorescent respond reached after 20 min (Fig. S8).

Fluorescence titration experiments were monitored for the Cu NASs with gradually increasing the concentration of Pb^{2+} ions. As shown in Fig. 5a and b, the fluorescence intensity of G1-Ste13-Cu NASs gradually decreased with increasing Pb^{2+}

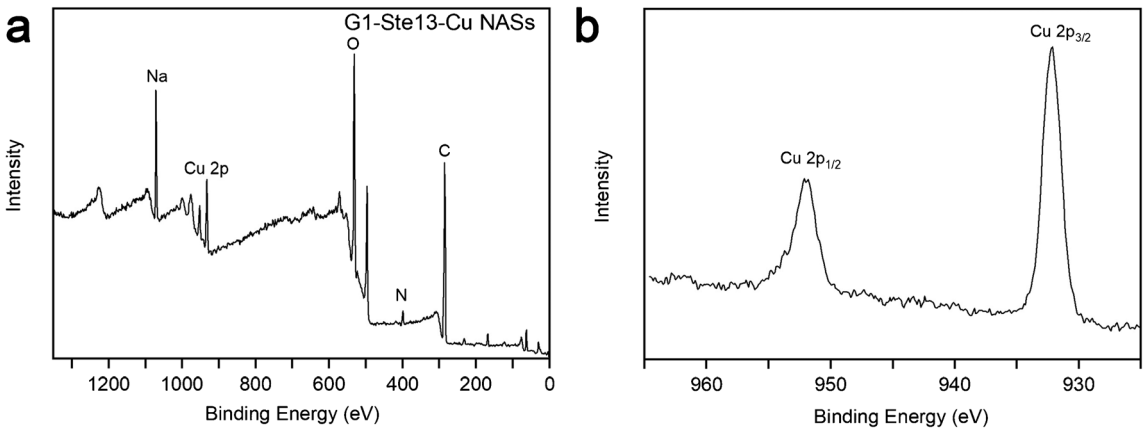

Fig. 6 **a** XPS full spectrum of G1-Ste13-Cu NASs. **b** XPS expanded spectrum of Cu 2p of G1-Ste13-Cu NASs

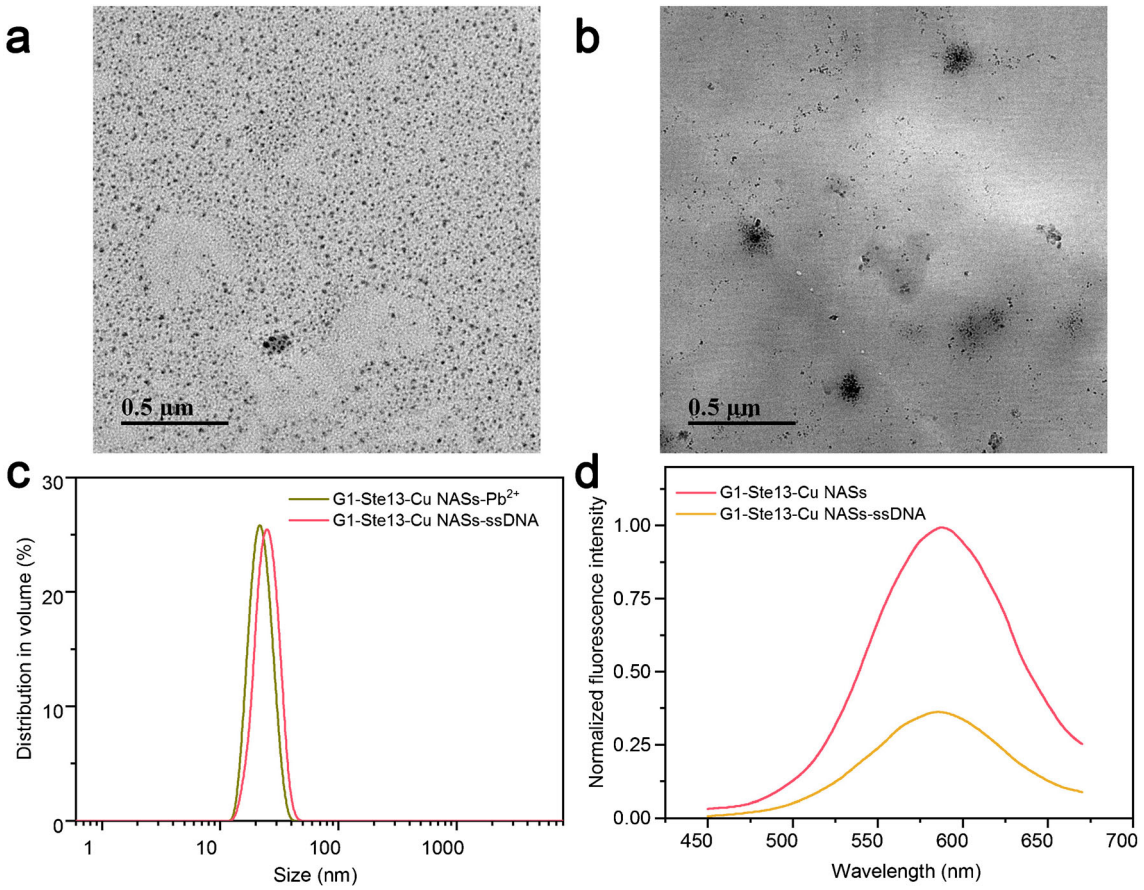

Fig. 7 TEM images of G1-Ste13-Cu NASs **a** with Pb^{2+} (200 nM) and **b** with ssDNA (3 μM). **c** Size measurement of G1-Ste13-Cu NASs with Pb^{2+}(200 nM) or with ssDNA (3 μM). **d** Fluorescence of G1-Ste13-Cu NASs with and without ssDNA

concentration and levelled off at 100–600 nM Pb^{2+}. As depicted in Fig. 5b, a linear response between the fluorescence intensity of G1-Ste13-Cu NASs and Pb^{2+} concentration was observed over the range of 2.0–100 nM, and the corresponding linear equation was F = 921.7–5.3028 C with a correlation coefficient of R^2 = 0.9952. The limit of detection (LOD), calculated following the signal-to-noise ratio of 3:1 (the IUPAC criteria), was estimated to be 0.75 nM. The limit of detection (LOD) is remarkably lower than the maximum recommended Pb^{2+} concentration (72 nM) by the US Environmental Protection Agency (EPA) [33] in drinking water

Table 1 Determination of Pb^{2+} in FBS samples (n = 3)

Sample	Added (μM)	Detected (μM)	Recover (%)	RSD (%)
1	0	ND (not detected)	/	/
2	0.1	0.092	92.0	3.5
3	0.4	0.386	96.5	2.0
4	1.6	1.458	91.1	3.4

The responses of G1-Ste13-Cu NASs to various heavy metal ions were tested. It was found that the fluorescent G1-Ste13-Cu NASs was significantly quenched by 0.3 μM Pb^{2+}, while the respond to the other metal ions even at 3 μM was negligible (Fig. S9). These results demonstrated the high potential of the G1-Ste13-Cu NASs as a highly sensitive and selective probe for Pb^{2+}. Pb^{2+} ions can react with Cu^+ through strong $5d^{10}(Pb^{2+})$-$3d^{10}(Cu^+)$ metalophilic interactions, which lead to the deposition of Pb atoms/ions on G1-Ste13-Cu NASs. The selectivity of sensing Pb^{2+} ions was mainly due to the two reasons: (1) this kind of metalophilic interaction did not exist between some common metal ions and Cu^+ ion; (2) only when this kind of metalophilic interaction was strong enough, dissociation of single-stranded nucleic acid from G1-Ste13-Cu NCs happened. Among the fluorescent metal NC-based detections of Pb^{2+}, the proposed Cu NAS-based fluorescent method was the most sensitive. Compared with some typical fluorescent detection methods (Table S4), the sensitivity of the proposed Cu NAS-based fluorescent method was comparable. Although the sensitivity of our Cu NAS-based method was lower than the methods integrating signal amplification strategies [34], it was much simple and rapid. In addition, the DNA dendrimer–templated Cu NASs have the

potential to be applied in cell image since DNA dendrimer possesses good fluorescence stability.

Mechanism of Pb^{2+} sensing

Due to the reduction of AA, rich Cu^{+} species would exist on the surface of dendrimer DNA-Cu NASs. As shown in Fig. 6a and b, the XPS peaks at 932.3 eV and 951.9 eV were assigned to 2p3/2 and 2p1/2 features of Cu(0) or Cu(I), which were similar with the results in the previous works on the preparation of dsDNA-templated Cu NCs [20, 35, 36]. Pb^{2+} ions could react with Cu^{+} via strong $5d^{10}(Pb^{2+})$-$3d^{10}(Cu^{+})$ metallophilic interaction, and this aurophilic interaction causes Pb atoms/ions to become deposited on the particle [37], which was considered as the main mechanism of the fluorescence quenching of dsDNA-templated Cu NCs by Pb^{2+} ions [38, 39]. The similar surface chemical state of the dendrimer DNA-Cu NASs with dsDNA-templated Cu NCs indicated that the above mechanism also existed in the dendrimer DNA-Cu NASs.

Moreover, the G1-Ste13-Cu NASs could be transformed into much smaller and monodisperse Cu NCs after incubated with 200 nM Pb^{2+} ions (Fig. 7a). The average size was 22 nm by DLS measurement (Fig. 7c), which was close to the size of G1-Ste0-Cu NASs (19 nm). In order to investigate the reason why the particle size of G1-Ste13-Cu NASs becomes similar to that of G0-Ste13-Cu NASs after adding Pb^{2+} to the system, a ssDNA (3 μM) complementary with the single-stranded end of the template G1-Ste13 was mixed with the G1-Ste13-Cu NASs. The obtained G1-Ste13-Cu NASs became much smaller with the average size of 26 nm by DLS measurement (Fig. 7b and Fig. 7c), which is similar to the particle size of G1-Ste13-Cu NASs after incubated with Pb^{2+}. And the fluorescence obviously decreased after the ssDNA was added (Fig. 7d). The ssDNA can be complementary to the end strand of the nucleic acid template of G1-Ste13-Cu NASs, destroying the van der Waals forces between the ssDNA and the G1-Ste13-Cu NCs [23].

The above disassembly of G1-Ste13-Cu NASs induced by ssDNA hybridization further confirmed that the sticky end of DNA template played a vital role in the assembly of the above DNA-Cu NMs and fluorescent sensing of Pb^{2+} ions. The above mechanism is shown in Fig. 1.

Real sample analysis

To test the practicality of the sensing systems in complex samples, the Cu NASs were further applied to detect Pb^{2+} ions in FBS, a complex biological matrix. Before the Pb^{2+} detection, the blank of the FBS was first detected, and no Pb^{2+} was detected. The FBS sample was spiked with 5.0, 20, and 80 nM of Pb^{2+} and then analyzed by using G1-Ste13-Cu NASs as the probe. The detection results are listed in Table 1. The recovery range of 91.1–96.5% with relative standard deviation (RSD) values less than 4.0% was achieved, demonstrating good accuracy and precision of this method. According to the US Environmental Protection Agency (USEPA), the maximum acceptable concentration for lead in blood is 480 nM [40]. We added 100 nM and 400 nM Pb^{2+} (both less than 480 nM) to serum, which can be detected with recoveries higher than 92%. Thus, these results proved that the probe can meet the need of actual sample detection. The background fluorescence in the serum will limit the application of nanocluster probes to some extent. However, appropriate dilution of serum could overcome this limitation

Conclusions

In this study, highly fluorescent Cu NASs were prepared using DNA dendrimers with sticky end as template for the first time. The sticky end of the DNA dendrimers could significantly affect the size, fluorescent intensity, and stability of the Cu NASs. The fluorescent enhancement of the Cu NASs was ascribed to AIEE effect derived from the self-assembly of the DNA dendrimers-Cu NCs. Due to the sensitive and rapid respond to Pb^{2+} as well as excellent stability in biological matrix, the proposed fluorescent Cu NASs demonstrated highly applicable potential as an excellent fluorescent probe for Pb^{2+} in complex samples. In addition, considering the high stability of the DNA dendrimer Cu NASs, they also were expected to be further used in various labelling analysis including fluorescent-labelled immunoassay, aptamer biosensor and cell image, etc.

Supplementary Information The online version contains supplementary material available at https://doi.org/10.1007/s00604-021-04967-y.

Acknowledgements The authors would like to thank Professor Xiao-Fang Shen of Jiangnan University for his valuable comments and advice in the preparation this paper. The work was supported by the National Natural Science Foundation of China (31871879), the National Key Research and Development Program (2018YFC1604400), and the National Key Research and Development Program (2019YFC1605405).

Declarations

Conflict of interest The authors declare no competing interests.

References

1. Truttmann V, Herzig C, Illes I, Limbeck A, Pittenauer E, Stoger-Pollach M, Allmaier G, Burgi T, Barrabes N, Rupprechter G (2020) Ligand engineering of immobilized nanoclusters on surfaces: ligand exchange reactions with supported $Au_{11}(PPh_3)_7Br_3$. Nanoscale 12:12809–12816. https://doi.org/10.1039/c9nr10353h

2. Agans RT, Dymond CE, Jimenez RE, Bunce NJ, Perry KJ, Salisbury RL, Hussain SM, Gupta RK, Karna SP (2020) Human nontumorigenic microglia synthesize strongly fluorescent Au/Fe nanoclusters, retaining bioavailability. ACS Omega 5:20983–20990. https://doi.org/10.1021/acsomega.0c02455
3. Baghdasaryan A, Besnard C, Lawson Daku LM, Delgado T, Burgi T (2020) Thiolato Protected copper sulfide cluster with the tentative composition $Cu_{74}S_{15}$(2-PET)$_{45}$. Inorg Chem 59:2200–2208. https://doi.org/10.1021/acs.inorgchem.9b02828
4. Deng HH, Shi XQ, Wang FF, Peng HP, Liu AL, Xia XH, Chen W (2017) Fabrication of water-soluble, green-emitting gold nanoclusters with a 65% photoluminescence quantum yield via host-guest recognition. Chem Mater 29:1362–1369. https://doi.org/10.1021/acs.chemmater.6b05141
5. Maity S, Bain D, Patra A (2019) Engineering atomically precise copper nanoclusters with aggregation induced emission. J Phys Chem C 123:2506–2515. https://doi.org/10.1021/acs.jpcc.8b09467
6. Gu Y, Zhao Z, Su H, Zhang P, Liu J, Niu G, Li S, Wang Z, Kwok RTK, Ni XL, Sun J, Qin A, Lam JWY, Tang BZ (2018) Exploration of biocompatible AIEgens from natural resources. Chem Sci 9:6497–6502. https://doi.org/10.1039/c8sc01635f
7. Zhou T, Zhu J, Gong L, Nong L, Liu J (2019) Amphiphilic block copolymer-guided in situ fabrication of stable and highly controlled luminescent copper nanoassemblies. J Am Chem Soc 141:2852–2856. https://doi.org/10.1021/jacs.8b12026
8. Li J, Hu X, Zhou Y, Zhang L, Ge Z, Wang X, Xu W (2019) β-Cyclodextrin-stabilized Au nanoparticles for the detection of butyl benzyl phthalate. ACS Appl Nano Mater 2:2743–2751. https://doi.org/10.1021/acsanm.9b00258
9. You JG, Tseng WL (2019) Peptide-induced aggregation of glutathione-capped gold nanoclusters: a new strategy for designing aggregation-induced enhanced emission probes. Anal Chim Acta 1078:101–111. https://doi.org/10.1016/j.aca.2019.05.069
10. Guo Y, Tong X, Ji L, Wang Z, Wang H, Hu J, Pei R (2015) Visual detection of Ca^{2+} based on aggregation-induced emission of Au(I)-Cys complexes with superb selectivity. Chem Commun 51:596–598. https://doi.org/10.1039/c4cc07592g
11. Su X, Liu J (2017) pH-guided self-assembly of copper nanoclusters with aggregation-induced emission. ACS Appl Mater Interfaces 9:3902–3910. https://doi.org/10.1021/acsami.6b13914
12. Qing T, Zhang K, Qing Z, Wang X, Long C, Zhang P, Hu H, Feng B (2019) Recent progress in copper nanocluster-based fluorescent probing: a review, Microchim. Acta 186. https://doi.org/10.1007/s00604-019-3747-4
13. Liu R, Wang CQ, Hu JY, Su YY, Lv Y (2018) DNA-templated copper nanoparticles: versatile platform for label-free bioassays. Trends Anal Chem 105:436–452. https://doi.org/10.1016/j.trac.2018.06.003
14. Wang HB, Zhang HD, Chen Y, Huang KJ, Liu YM (2015) A label-free and ultrasensitive fluorescent sensor for dopamine detection based on double-stranded DNA templated copper nanoparticles. Sensors Actuators B Chem 220:146–153. https://doi.org/10.1016/j.snb.2015.05.055
15. Cao Q, Li J, Wang EK (2019) Recent advances in the synthesis and application of copper nanomaterials based on various DNA scaffolds. Biosens Bioelectron 132:333–342. https://doi.org/10.1016/j.bios.2019.01.046
16. Kim S, Kim JH, Kwon WY, Hwang SH, Cha BS, Kim JM, Oh SS, Park KS (2019) Synthesis of DNA-templated copper nanoparticles with enhanced fluorescence stability for cellular imaging. Microchim Acta 186:5. https://doi.org/10.1007/s00604-019-3620-5
17. Ran X, Wang ZZ, Pu F, Ju EG, Ren JS, Qu XG (2021) Nucleic acid-driven aggregation-induced emission of Au nanoclusters for visualizing telomerase activity in living cells and in vivo dagger. Materials Horizons 7:1769–1775. https://doi.org/10.1039/d0mh01875a
18. Ouyang X, Wang M, Guo L, Cui C, Liu T, Ren Y, Zhao Y, Ge Z, Guo X, Xie G, Li J, Fan C, Wang L (2020) DNA nanoribbon-templated self-assembly of ultrasmall fluorescent copper nanoclusters with enhanced luminescence, Angew. Chem, Int Ed Engl 59:11836–11844. https://doi.org/10.1002/anie.202003905
19. Meng HM, Zhang X, Lv Y, Zhao Z, Wang NN, Fu T, Fan H, Liang H, Qiu L, Zhu G, Tan W (2014) DNA dendrimer: an efficient nanocarrier of functional nucleic acids for intracellular molecular sensing. ACS Nano 8:6171–6181. https://doi.org/10.1021/nn5015962
20. Chen J, Liu J, Fang Z, Zeng L (2012) Random dsDNA-templated formation of copper nanoparticles as novel fluorescence probes for label-free lead ions detection. Chem Commun 48:1057–1059. https://doi.org/10.1039/c2cc16668b
21. Wang JX, Li J, Li Y, Zhang ZJ, Wang L, Wang D, Su L, Zhang XJ, Tang BZ (2020) pH-responsive Au(I)-disulfide nanoparticles with tunable aggregation-induced emission for monitoring intragastric acidity. Chem Sci 11:6472–6478. https://doi.org/10.1039/d0sc01843k
22. Li Q, Mosquera MA, Jones LO, Parakh A, Chai JS, Jin RC, Schatz GC, Gu XW (2020) Pressure-induced optical transitions in metal nanoclusters. ACS Nano 14:11888–11896. https://doi.org/10.1021/acsnano.0c04813
23. Li H, Rothberg L (2004) Colorimetric detection of DNA sequences based on electrostatic interactions with unmodified gold nanoparticles. Proc Natl Acad Sci U S A 101:14036–14039. https://doi.org/10.1073/pnas.0406115101
24. Li J, Fu W, Bao J, Wang Z, Dai Z (2018) Fluorescence regulation of copper nanoclusters via DNA template manipulation toward design of a high signal-to-noise ratio biosensor. ACS Appl Mater Interfaces 10:6965–6971. https://doi.org/10.1021/acsami.7b19055
25. Rajamanikandan R, Ilanchelian M (2018) Protein-protected red emittive copper nanoclusters as a fluorometric probe for highly sensitive biosensing of creatinine. Anal Methods 10:3666–3674. https://doi.org/10.1039/c8ay00827b
26. Wu Z, Liu J, Gao Y, Liu H, Li T, Zou H, Wang Z, Zhang K, Wang Y, Zhang H, Yang B (2015) Assembly-induced enhancement of Cu nanoclusters luminescence with mechanochromic property. J Am Chem Soc 137:12906–12913. https://doi.org/10.1021/jacs.5b06550
27. Wang WX, Wu Y, Li HW (2017) Regulation on the aggregation-induced emission (AIE) of DNA-templated silver nanoclusters by BSA and its hydrolysates. J Colloid Interface Sci 505:577–584. https://doi.org/10.1016/j.jcis.2017.06.033
28. Liu Y, Yao D, Zhang H (2018) Self-assembly driven aggregation-induced emission of copper nanoclusters: a novel technology for lighting. ACS Appl Mater Interfaces 10:12071–12080. https://doi.org/10.1021/acsami.7b13940
29. Nsibande SA, Forbes PBC (2019) Development of a quantum dot molecularly imprinted polymer sensor for fluorescence detection of atrazine. Luminescence 34:480–488. https://doi.org/10.1002/bio.3620
30. Hu X, Liu X, Zhang X, Chai H, Huang Y (2018) One-pot synthesis of the CuNCs/ZIF-8 nanocomposites for sensitively detecting H_2O_2 and screening of oxidase activity. Biosens Bioelectron 105:65–70. https://doi.org/10.1016/j.bios.2018.01.019
31. Qu Y, Ju Y, Cortez-Jugo C, Lin Z, Li S, Zhou J, Ma Y, Glab A, Kent SJ, Cavalieri F, Caruso F (2020) Template-mediated assembly of DNA into microcapsules for immunological modulation. Small: e2002750. https://doi.org/10.1002/smll.202002750
32. Wei X, Tian T, Jia S, Zhu Z, Ma Y, Sun J, Lin Z, Yang CJ (2015) Target-responsive DNA hydrogel mediated "stop-flow" microfluidic paper-based analytic device for rapid, portable and

visual detection of multiple targets. Anal Chem 87:4275–4282. https://doi.org/10.1021/acs.analchem.5b00532

33. Kim JH, Han SH, Chung BH (2011) Improving Pb^{2+} detection using DNAzyme-based fluorescence sensors by pairing fluorescence donors with gold nanoparticles. Biosens Bioelectron 26: 2125–2129. https://doi.org/10.1016/j.bios.2010.09.018
34. Chen XL, Wang XF, Lu Z, Luo HB, Dong L, Ji Z, Xu FL, Huo DQ, Hou CJ (2020) Ultra-sensitive detection of Pb^{2+} based on DNAzymes coupling with multicycle strand displacement amplification (M-SDA) and nano-graphene oxide. Sensors Actuators B Chem 311:127898. https://doi.org/10.1016/j.snb.2020.127898
35. Ghosh R, Sahoo AK, Ghosh SS, Paul A, Chattopadhyay A (2014) Blue-emitting copper nanoclusters synthesized in the presence of lysozyme as candidates for cell labeling. ACS Appl Mater Interfaces 6:3822–3828. https://doi.org/10.1021/am500040t
36. Ye T, Peng Y, Yuan M, Cao H, Yu JS, Li Y, Xu F (2019) Target-induced in-situ formation of fluorescent DNA-templated copper nanoparticles by a catalytic hairpin assembly: application to the determination of DNA and thrombin. Microchim Acta 186:760. https://doi.org/10.1007/s00604-019-3927-2
37. Huang YQ, Yang LN, Wang YS, Xue JH, Chen SH (2018) Protamine-stabilized gold nanoclusters as a fluorescent nanoprobe for lead(II) via Pb(II)-Au(I) interaction. Microchim Acta 185:483. https://doi.org/10.1007/s00604-018-3019-8
38. Deng HH, Fang XY, Huang KY, He SB, Peng HP, Xia XH, Chen W (2019) Regulation of metal ion selectivity of fluorescent gold nanoclusters by metallophilic interactions. Anal Chim Acta 1088: 116–122. https://doi.org/10.1016/j.aca.2019.08.047
39. Xie J, Zheng Y, Ying JY (2010) Highly selective and ultrasensitive detection of Hg^{2+} based on fluorescence quenching of Au nanoclusters by Hg^{2+}-Au^{+} interactions. Chem Commun 46:961–963. https://doi.org/10.1039/b920748a
40. Xu W, Zhao A, Zuo F, Khan R, Hussain HMJ, Li J (2020) A highly sensitive DNAzyme-based SERS biosensor for quantitative detection of lead ions in human serum. Anal Bioanal Chem 412:4565–4574. https://doi.org/10.1007/s00216-020-02709-2